PNAS
www.pnas.org

Supplementary Information for

Priming of microglia with IFN-γ slows neuronal gamma oscillations in situ

Thuy-Truc Ta, Hasan Onur Dikmen, Simone Schilling, Bruno Chausse, Andrea Lewen, Jan-Oliver Hollnagel and Oliver Kann

Corresponding author: Oliver Kann
Email: oliver.kann@physiologie.uni-heidelberg.de

This PDF file includes:

Supplementary text (SI Discussion, SI Materials and methods, SI References)
Supplementary figures (SI Figs. S1 to S7)

SI Discussion

Use of slice cultures in experimental neuroscience

Organotypic hippocampal slice cultures have been increasingly used to study neuronal activity, energy metabolism and microglial activation *in situ* (Ajmone-Cat et al., 2013; Bahr et al., 1995; Duport and Garthwaite, 2005; Fischer et al., 2002; Hailer et al., 1996; Kann et al., 2003; Neumann et al., 1996; Papageorgiou et al., 2016; Stoppini et al., 1991; Vinet et al., 2012).

Non-activated microglia in control (untreated) slice cultures

We are confident that microglia in our control slice cultures are non-activated or, if at all, feature only very low levels of priming/activation for the following reasons: First, microglia show a ramified morphology and their territories do widely not overlap (Fig. 1B). Second, microglia respond with morphological changes and proliferation to IFN-γ and LPS exposures (Fig. 1B and C and Papageorgiou et al., 2016). Third, microglia show low levels of activation markers, such as MHC-II and CD86 (Fig. 1D and E, SI Appendix, Fig. S1). Fourth, release of IL-6 and TNF-α is very low (Fig. 2A). Fifth, iNOS expression (mRNA and protein level) and NO release are very low (Fig. 2B-D, SI Appendix, Fig. S2B and C). Sixth, different microglial activation stages with gradual upregulation of activation markers (e.g., iNOS, IL-6) and gradual effects on neuronal function and survival can be reliably induced using IFN-γ, LPS and IFN-γ+LPS (IFN-γ→LPS) (Fig. 1, Fig. 2 and SI Appendix, Fig. S1, S2 and S4). Seventh, physiological gamma oscillations that are exquisitely sensitive to metabolic and oxidative stress can be reliably evoked in control slice cultures (Kann, 2016; Schneider et al., 2015). Eighth, the single exposure to LPS of up to 10 μg/ml (SI Appendix, Fig. S4 and Papageorgiou et al., 2016) has either no or only minor effects on neuronal activity and survival in slice cultures, which widely excludes a primed microglial phenotype due to trauma (cutting of slices) and the presence of horse serum that is mandatory for the high quality of slice cultures (Kann et al., 2011; Schneider et al., 2015).

These microglial characteristics are in line with other reports on slice cultures (Ajmone-Cat et al., 2013; Duport and Garthwaite, 2005; Hailer et al., 1996; Neumann et al., 1996; Vinet et al., 2012). However, ramified microglia in control slice cultures might still differ from ‘surveying’ microglia in the healthy brain (Hanisch and Kettenmann, 2007; Ransohoff and Perry, 2009).

Entry of IFN-γ to the brain parenchyma

We show that IFN-γ priming induces substantial proliferation and moderate activation of microglia that is capable to slow neural information processing. This mechanism might contribute to cognitive impairment in chronic brain disease, well before neurodegeneration occurs (Frere and Slutsky, 2018; Klein et al., 2017; Mably and Colgin, 2018). IFN-γ is predominantly released from T helper type 1 (Th1) cells, cytotoxic T lymphocytes and natural killer cells (Colton, 2009; Mosser and Edwards, 2008).

Several pathways have been identified and discussed, through which IFN-γ might enter (or signal to) the brain parenchyma and thus serve in microglial priming. First, there is experimental evidence that peripheral IFN-γ can enter the CNS through the blood-brain barrier in normal mice (Pan et al., 1997), and indeed the intravenous application of IFN-γ in normal adult rats resulted in activation of microglial and endothelial cells in the brain (Grau et al., 1997). Second, peripheral IFN-γ might have facilitated entry to the brain parenchyma when the blood-brain barrier gets (transiently) leaky, e.g., in aging, stroke, multiple sclerosis and Alzheimer's disease (Bell and Zlokovic, 2009; Daneman and Prat, 2015; Dendrou et al., 2015; Montagne et al., 2015; Prinz and Priller, 2017; van de Haar et al., 2016). Third, IFN-γ can be released from T lymphocytes and natural killer cells that infiltrate the brain parenchyma (Colton, 2009; Lynch et al., 2014). Elevated IFN-γ levels and/or T cell infiltration have been reported during acute infections (Kothur et al., 2016; McManus and Heneka, 2017) and in patients with multiple sclerosis (Giunti et al., 2003; Heesen et al., 2006), Alzheimer's disease (Monson et al., 2014; Rogers et al., 1988; Togo et al., 2002), depression (Inserra et al., 2018) and schizophrenia (Miller et al., 2011; Na et al., 2014).

However, further research is required to clarify the role of IFN-γ-primed microglia, iNOS upregulation, and low-grade inflammation in chronic neurologic and psychiatric disorders in humans (Ding et al., 1997; Hoos et al., 2014; Lee et al., 1993; Peterson et al., 1994).

NO in the regulation of neuronal (dys)function

Nitric oxide (NO) can be generated by endothelial (eNOS), neuronal (nNOS), and inducible (iNOS) (Feil and Kleppisch, 2008). For NO as a signaling molecule, three main routes of action have been discussed, i.e. through nitrosothiol production, cGMP and protein kinase G (PKG) (Hardingham et al., 2013). Using these pathways, NO is capable to regulate synaptic transmission in excitatory and inhibitory neurons. Important targets in this regulation are Munc18 and Syntaxin 1A as well as ion channels, such as NMDA and $GABA_A$ receptors, N-type Ca^{2+} channels, cyclic nucleotide-gated (CNG) and hyperpolarization-activated cyclic nucleotide-gated (HCN) channels (Arancio et al., 1996; Dejanovic and Schwarz, 2014; Feil and Kleppisch, 2008; Gasulla and Calvo, 2015; Hardingham et al., 2013; Johnstone and Raymond, 2011; Lange et al., 2012; Neitz et al., 2014; Szabadits et al., 2007; West et al., 2002).

Moreover, NO is capable to reversibly inhibit cytochrome *c* oxidase and, thus, mitochondrial energy production in neurons and astrocytes (Bolaños et al., 1994; Bolaños et al., 2008; Brorson et al., 1999; Brown and Cooper, 1994; Brown and Neher, 2010; Cleeter et al., 1994).

NO can also induce neuronal dysfunction in synergy with superoxide anion that is generated during physiological neuronal respiration and through NADPH oxidase of activated phagocytes (Brown and Vilalta, 2015; Kann, 2016; Lipton et al. 1993; Morán et al., 2012; Wink et al., 1993). However, IFN-γ widely failed to induce the production of reactive oxygen species in microglia, at least, *in vitro* (Colton et al., 1992; Hu et al., 1995; Pawate et al., 2004; Spencer et al., 2016; but see Herrera-Molina et al., 2012).

Whether the slowing of gamma oscillations reported in our study reflects direct and/or synergistic NO-mediated alterations in the intrinsic biophysical properties of neurons, glutamatergic and $GABA_A$-receptor mediated neurotransmission and/or energy metabolism needs to be explored in intact hippocampal tissue, particularly at pyramidal cell-basket cell and basket cell-pyramidal cell synapses (Kann, 2016).

Disturbed gamma oscillations in Alzheimer's disease

In several rodent animal models of Alzheimer's disease, disturbances of 'slow' gamma oscillations (~25-55 Hz) have been described (Gillespie et al., 2016; Mably et al., 2017; Mably

and Colgin, 2018). And it has been hypothesized that such disturbances, especially in the hippocampus and the entorhinal cortex, might contribute to early cognitive symptoms that include impairments of episodic and spatial memory (Hyman et al., 1997; McKhann et al., 2011; Roy et al., 2016). However, the molecular and cellular mechanisms (e.g., altered calcium, energy, redox and immune homeostasis) underlying such disturbances are far from being understood (Kann, 2016; Frere and Slutsky, 2018; Mably and Colgin, 2018).

Based on findings in animal models and patients, it has been proposed that the significant increase in microglial activation induces inflammatory neuronal dysfunction and neurodegeneration in Alzheimer's disease, mainly by the release of proinflammatory cytokines (Ransohoff, 2016; McManus and Heneka, 2017). In that, microglial activation is thought to be triggered by a variety of factors that comprise amyloid-β deposition, blood-brain barrier leakage, T cell infiltration, plaque-associated pathogens as well as inflammatory events occurring in the periphery, such as respiratory infection (McManus et al., 2014; McManus and Heneka, 2017).

Here, we provide solid experimental evidence that even moderate microglial activation (priming) with IFN-γ is sufficient to slow neuronal gamma oscillations through moderate upregulation of iNOS and NO release. It is of high interest for basic neuroscientists, neuroimmunologists and clinicians to study the impact of other microglial activation scenarios (e.g., ligands of different Toll-like receptors) on neuronal network dysfunction.

SI Materials and methods

Ethical statement

Rats were purchased from Charles-River (Sulzfeld, Germany) and handled in accordance with the European directive 2010/63/EU and with consent of the animal welfare officers at University of Heidelberg (licenses, T46/14 and T96/15). Experiments were performed and reported in accordance with the ARRIVE guidelines.

Preparation of slice cultures

Organotypic hippocampal slice cultures were prepared as described (Kann et al., 2011; Papageorgiou et al., 2016). In brief, hippocampal slices (400 µm) were cut with a McIlwain tissue chopper (Mickle Laboratory Engineering Company Ltd., Guildford, UK) from 9- to 10-day-old male Wistar rats under sterile conditions. Three to five slices with intact hippocampal structures were maintained on a Biopore™ membrane (Millicell standing inserts, Merck Millipore, Darmstadt, Germany) between culture medium, which consisted of 50% minimal essential medium, 25% Hank's balanced salt solution (Sigma-Aldrich, Taufkirchen, Germany), 25% heat-inactivated horse serum (Life Technologies, Darmstadt, Germany), and 2 mM L-glutamine (Life Technologies) at pH 7.3 titrated with Trisbase, and humidified normal atmosphere enriched with 5% (vol/vol) CO_2 (36.5°C) in an incubator (Heracell, Thermoscientific, Dreieich, Germany). The calculated glucose concentration in the culture medium was about 4 mM (Schneider et al., 2015); the partial oxygen pressure (pO_2) in the slice core ranges between 47 mmHg and 18 mmHg, depending on the neuronal network activity state (Huchzermeyer et al., 2013). These values are close to the physiological range (Schneider et al., 2017). The culture medium (1 ml) was replaced three times per week.

Exposures of slice cultures and microglial depletion with clodronate

Exposures to IFN-γ or IFN-γ plus LPS started on day in vitro (DIV) 7 for 72 h, or selectively for 24 h as indicated, without medium exchange. From each preparation, membranes with slice cultures were randomly assigned to experimental groups. At the end of exposures, slice cultures

were used for electrophysiological recordings, fixed for immunohistochemistry or frozen for RNA isolation. For biochemical analysis, the culture medium was stored at -80°C. Liposome-containing medium was centrifuged.

For microglial priming, we used different concentrations of recombinant IFN-γ (PeproTech GmbH, Hamburg, Germany). As second inflammatory stimulus, we used LPS from Escherichia coli, serotype R515 (Re) (Alexis Biochemicals, Enzo Life Sciences GmbH, Lörrach, Germany). Stock solutions of IFN-γ were prepared in 10 mM sterile sodium phosphate and further diluted in culture medium. LPS was ready-to use. Aliquots were kept at -20°C.

Chemical depletion of microglia from slice cultures was made with liposome-encapsulated clodronate (Liposoma B.V., Amsterdam, The Netherlands) (Vinet et al., 2012). Liposome-encapsulated clodronate at a final concentration of 100 µg/ml was present in the culture medium from DIV 0 on and during the exposures to IFN-γ (Papageorgiou et al., 2016).

Biochemical analysis

All enzyme-linked immunosorbent assay (ELISA) kits were purchased from R&D (R&D Systems, Inc., Minneapolis, MN, USA) and applied according to the supplier´s protocol for the detection of interleukin 6 (IL-6; Cat. num. DY506) and tumor necrosis factor alpha (TNF-α; Cat. num. 510). Concentrations of antibodies strictly followed the suppliers protocol. Wash buffer consisted of 0.05% Tween 20 (Merck-Millipore; Darmstadt, Germany) in PBS. Capture antibodies were diluted in PBS (pH 7.2-7.4) and the reactions plate was coated overnight. The detection antibody for TNF-α was diluted in the reagent dilutent (RD), consisting of 1% bovine serum albumin in PBS (pH 7.2-7.4); the detection antibody for Il-6 was diluted in 2% normal goat serum (NGS) in RD. Ten-point standard curves were constructed from nine sequential two-fold dilution steps of recombinant IL-6 (8000 pg/ml) or TNF-α (4000 pg/ml), and a negative control containing only non-treated culture medium. Samples were incubated in the coated reaction plate for 2 h. The detection antibody was then applied for 2 h and visualized with tetramethylbenzidine substrate solution (Moss Inc., Pasadena, USA). The development reaction was stopped with sulphuric acid, and the optical density (OD) was determined with a microplate reader (iMark Microplate Absorbance Reader, Bio-Rad Laboratories GmbH, Munich, Germany)

at 450 nm (with 540 nm reference). The concentrations of TNF-α and IL-6 (pg/ml) was estimated by using the quadratic fit.

Griess reaction

Nitric oxide release was quantified by determining the levels of the stable metabolite nitrite using a Griess reaction-based assay that was carried out with undiluted culture medium. Nine-point standard curves were constructed by two-fold dilution steps of an 80 μM sodium nitrite high standard (Merck Chemicals, Darmstadt, Germany). After addition of the Griess reagent mixture (0.05% 1-naphthylethylenediamine hydrochloride, 0.5% sulfanilamide and 2.5% orthophosphoric acid), the optical density was measured in a microplate reader at 540 nm (Bio-Rad). The molarity of NO (μM) was calculated from the standard curve using linear fit.

RNA isolation and qRT-PCR

To determine the expression of target genes, five slice cultures per Biopore™ membrane were considered as a single sample for RNA isolation. RNA was isolated using RNeasy® Plus Mini kit (Qiagen, Hilden, Germany) followed by cDNA synthesis by High Capacity cDNA Reverse Transcription kit (Applied Biosystems, Foster City, CA, USA), both according to the manufacturer's instructions. The synthesized cDNA was used as a template for qPCR amplification carried by the StepOnePlus™ Real-Time PCR System (Applied Biosystems, Foster City, CA, USA). Each PCR reaction contained 20 ng of cDNA, 200 nM of TaqMan assays (MHC-II (CD74) - Rn00565062_m1, iNOS - Rn00561646_m1, ACTB - Rn00667869_m1, CD40 - Rn01423584_g1, CD80 - Rn00709368_m1), TaqMan Fast Advanced Master Mix and ribonuclease-free water to a final volume of 10 μl. Reaction conditions were 2 min at 50°C, 2 min at 95°C followed by 40 cycles of 1 sec at 95°C, 20 sec at 60°C. StepOnePlus™ software was used for comparative gene expression analysis, and β-actin was used as an endogenous control.

Stainings of slice cultures

Slice cultures were fixed for at least 2 h with 4% paraformaldehyde in 0.1 M phosphate buffered saline (PBS, pH 6.8), incubated for 2-3 h in 30% sucrose (AppliChem GmbH, Darmstadt, Germany) and cut into 25 or 30 µm sections with a cryostat (CM1850; Leica Microsystems). All stainings were conducted in free-floating sections. All primary antibodies were diluted in PBS + 0.3% Triton™ X-100 or PBS + 0.2% Triton™ X-100, including 10% normal goat or horse serum (Life Technologies). Secondary antibodies were either diluted in 0.2% bovine serum albumin (BSA) dissolved in PBS + 0.2% Triton™ X-100 for immunohistochemistry or in 2% normal goat serum (NGS) dissolved in PBS + 0.2% Triton™ X-100 for immunofluorescence. Several washing steps with PBS were conducted, e.g., after blocking of unspecific binding sites or antibody applications.

Immunohistochemistry

For immunohistochemistry of ionized calcium binding adaptor molecule 1 (Iba1), parvalbumin-positive (PV) interneurons and microtubule associated protein 2 (MAP2), unspecific immunoglobulin reactions were blocked for 1 h with 10% serum. Primary antibodies were rabbit polyclonal anti-Iba1 (Fujifilm-WAKO Chemicals Europe GmbH, Neuss, Germany), mouse monoclonal anti-MAP2 (Abcam, Cambridge, UK) and mouse anti-PV (Sigma-Aldrich) all diluted 1:1000; rabbit monoclonal anti-CD86 (Abcam) was diluted 1:500 and mouse monoclonal anti-MHC class II was diluted 1:250 (Abcam). Cryosections were exposed overnight to the primary antibody. Unspecific binding sites of the secondary antibodies were blocked for 1 h in 0.2% BSA (Carl Roth GmbH & Co. KG, Karlsruhe, Germany). Secondary antibodies used were: for Iba1 and CD86 stainings, biotin-conjugated goat anti-rabbit (Sigma-Aldrich) diluted 1:1000; for PV, MAP2 and MHC-II, biotin-conjugated horse anti-mouse (Vector Laboratories Inc., CA, USA) diluted 1:2000 or 1:1000 (MHC-II). The secondary antibody was applied overnight at 4°C under light protected conditions. Afterwards, sections were incubated for 2 h with 0.5% avidin and biotinylated horseradish peroxidase (Vectastain Elite ABC Kit, Vector Laboratories). Antibody binding was visualized by adding 0.05% diaminobenzidine substrate, 0.3% ammonium nickel sulphate in 0.05 M Trisbase 7-9® and 0.003% H_2O_2 for <5 min. Then the reaction was stopped by adding PBS (when the brown color was intense enough). Stained sections were placed on object plates and dried. Sections were then exposed to ascending ethanol series, for 10 min in

xylene (Sigma-Aldrich) and finally embedded with Entellan®Neu (Merck Millipore, Schwalbach, Germany).

For immunofluorescence of PV, CD68 (macrosialin, marker for monocytes and macrophages), CD11b (also known as OX42, Mac-1, activation marker) and iNOS (inducible nitric oxide synthase) unspecific binding sites of the first antibodies were blocked by 5% NGS. Primary antibodies were mouse anti-parvalbumin (Sigma-Aldrich), rabbit anti-CD68 (Abcam), mouse anti-CD11b (Serotec, Puchheim, Germany) and rabbit polyclonal anti-iNOS (Merck-Millipore Chemicals, Darmstadt, Germany), diluted 1:1000 (except anti-CD68, 1:500). Cryosections were exposed overnight to the primary antibody. The secondary antibodies, i.e., goat anti-mouse Alexa-568 (Life Technologies) and goat anti-rabbit atto-488 (Sigma-Aldrich), were applied for at least 90 min at 4°C under light protected conditions. Counterstaining of DNA (nuclei) was made with 4′,6-Diamidine-2′-phenylindole dihydrochloride (DAPI, dissolved in double-distilled water, Carl Roth). Sections were washed three-times in double-distilled water, placed on object plates and dried. Afterwards sections were embedded with fluorescent mounting medium (Agilent Technologies, Carpinteria, USA). Image analysis was done using Image J (Schneider et al., 2012).

Toluidine blue staining

For toluidine blue staining (Sigma-Aldrich), sections were mounted on slides, dried and exposed for at least 2h to 70% ethanol followed by descending ethanol series, briefly rinsed in double-distilled water and then incubated in 0.1% toluidine blue working solution (pH 2.3) for 1-5 min. Thereafter, the sections were briefly rinsed in double-distilled water. 96% ethanol with traces of glacial acetic acid was used for color differentiation of the staining. Sections were then exposed to 100% ethanol, followed by a 1:1 mixture of 100% ethanol and xylene and finally xylene for 3-10 min. Sections were embedded with Entellan®Neu (Merck Millipore, Schwalbach, Germany).

Stereological counting of microglia

The numbers of microglia (Iba1-positive cell somas) were estimated with design-based stereology recently described for hippocampal slice cultures in detail (SI Materials and methods,

Papageorgiou et al., 2016). In brief, we implemented the optical fractionator probe using the Stereoinvestigator® 5.65 software (MicroBrightField Europe, Delft, Netherlands), which provides an estimator of the total particle number in a three-dimensional structure. Sequential sections (total of 4-7) of each slice culture were included in the analysis. To satisfy the coefficient of sampling error (CE) <0.1, the optimal size of the frame associated area and grid spacing was chosen (Papageorgiou et al., 2016). The estimated microglia number of each slice culture, $\widehat{N}$, was determined using the optical fractionator equation, i.e. $\widehat{N} = \frac{Q}{hsf*asf*ssf}$. Q was the number of the counted cells in the fractionator frame associated area of all sections, *hsf* the height sampling fraction ($\frac{fractionator\ height}{section\ thickness}$), *asf* the area sampling fraction ($\frac{frame\ associated\ area}{contour\ area\ of\ all\ sections}$), *ssf* the section sampling fraction, i.e. interval of sections sampled through an object of interest. As we sampled every section of each slice culture, the section sampling fraction was always 1. As a result of inevitable tissue shrinkage during the staining procedures, the initial section thickness before staining (25 µm, obtained by cutting with a cryostat) had to be adjusted.

Due to very low cell numbers and irregular cell distribution in clodronate-treated slice cultures (microglial depletion), we defined the fractionator frame associated area as identical to the contour area of all sections in all clodronate-treated slice cultures, i.e. *asf = 1*. The estimated microglia number of each slice culture was determined using the optical fractionator equation. The counted cell number was corrected for tissue shrinkage (Papageorgiou et al., 2016). Initially, identification and counting of microglia was made independently by two of the authors, which resulted in similar cell numbers.

Recording solutions and drugs

Slice cultures were constantly supplied with pre-warmed recording solution (artificial cerebrospinal fluid, ACSF). ACSF contained 129 mM NaCl, 3 mM KCl, 1.25 mM NaH_2PO_4, 1.8 mM $MgSO_4$, 1.6 mM $CaCl_2$, 21 mM $NaHCO_3$ and 10 mM glucose (Kann et al., 2011; Papageorgiou et al., 2016). The pH was 7.3 when the recording solution was saturated with 95% O_2 and 5% CO_2. Recordings were done at 34 ± 1°C.

Gamma oscillations were elicited by continuous application of acetylcholine and the acetylcholine-esterase inhibitor physostigmine via the recording solution; this approach mimics cholinergic input to the hippocampus in vivo (Hájos and Paulsen, 2009). Cholinergic gamma oscillations in situ share many features with gamma oscillations in vivo and require both neuronal excitation and fast inhibition (Hájos and Paulsen, 2009; Kann et al., 2011; Kann, 2016).

Standard salts, acetylcholine and 1400W were purchased from Sigma-Aldrich, physostigmine was from Tocris (R&D Systems GmbH, Wiesbaden-Nordenstadt, Germany) and SNAP (S-Nitroso-N-Acetyl-D,L-Penicillamine) from Biomol (Hamburg, Germany).

Recordings of local field potentials

For electrophysiological recordings, the intact Biopore™ membrane carrying slice cultures was inserted into the recording chamber (Kann et al., 2011; Papageorgiou et al., 2016). Slice cultures were maintained at the interface between recording solution and ambient gas mixture. Intact Biopore™ membrane inserts ensure rapid and efficient supply of oxygen, energy substrates and drugs through the recording solution (rate 1.8 ml/min) that flows underneath. The interface condition permits constant oxygen supply from the ambient gas mixture (95% O_2 and 5% CO_2, rate 1.5 l/min).

The local field potential (LFP) was recorded with glass electrodes (resistance of 1-2 MOhm) that were made from GB150F-8P borosilicate filaments (Science Products GmbH, Hofheim, Germany) using a Zeitz DMZ Puller (Zeitz-Instruments Vertriebs GmbH; Martinsried, Germany), and filled with ACSF. The electrode was positioned in the stratum pyramidale of the CA3 region with a mechanical micromanipulator (MM 33, Märzhäuser, Wetzlar, Germany). Local field potentials were recorded with an EXT 10-2F amplifier in EPMS-07 housing (npi electronic GmbH, Tamm, Germany), low-pass filtered at 3 kHz, and digitized at 10 kHz using CED 1401 interface and Spike2 software (Cambridge Electronic Design, Cambridge, UK) for offline analysis.

Data analysis and statistics

Offline signal analysis of gamma oscillations was performed in MatLab 11.0 (The MathWorks, Inc., Natick, MA, USA). Data segments of 5 min were low-pass filtered with a digital Butterworth algorithm at 200 Hz corner frequency and processed with Welch´s algorithm with a Hamming window size of 4096 points for calculation of the power spectral density (PSD) (bin size = 2.441 Hz). Gamma oscillations were analyzed for various parameters, i.e., peak frequency (frequency, *f*), peak power (power), and full width at half-maximum (FWHM). Spectrograms (time-frequency plots) were derived from continuous wavelet transforms of a given local field potential recording using Morlet wavelets. This method provides an instant measure of the power of various frequencies at any given time point, thereby offering visualization of fast dynamics in frequency and power. Data are reported as mean ± SEM derived from slice cultures ('slices') (n) and independent preparations (N) of rat pups, unless stated otherwise. Statistical significance (*$P < 0.05$) was determined in GraphPad Prism® 6.0 (GraphPad Software, California, USA). Data distribution was tested for normality with the Shapiro-Wilk test. Statistical tests are specified in the figure legends. Figures were created with MatLab 15a, GraphPad Prism® 6.0 (GraphPad Software), and CorelDRAW (Corel, Ottawa, Ontario, Canada).

SI Figures

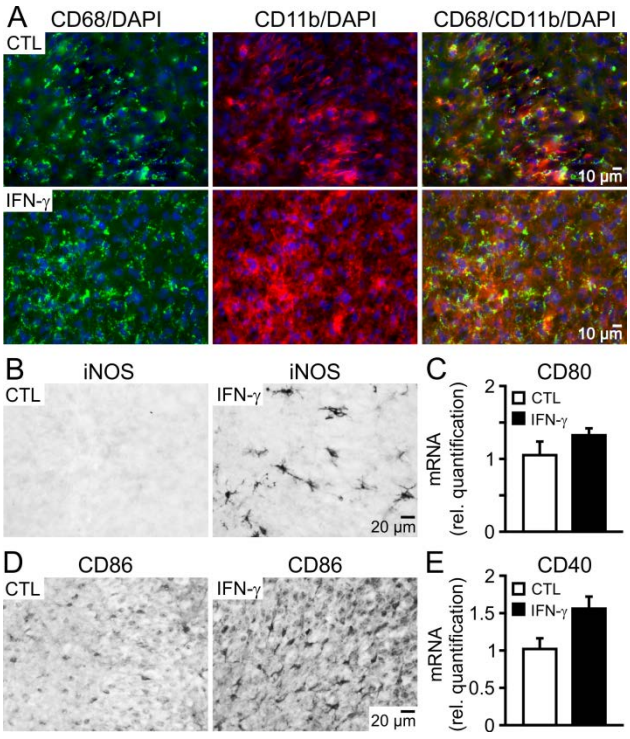

Fig. S1. IFN-γ activates microglia. Microglia were stained with markers in naive control (CTL) and slice cultures exposed to IFN-γ (1000 ng/ml). (*A*) Immunohistochemistry with general microglial markers, CD68 (green) and CD11b (red), and nuclear counterstaining with DAPI (blue) in CTL and IFN-γ. Note the moderate increase of fluorescence staining intensity in IFN-γ (lower images). (*B*) iNOS immunohistochemistry in CTL and IFN-γ. Note the moderate increase in iNOS-positive cell number in IFN-γ. (*C*) The levels of CD80 mRNA were determined in tissue homogenates pooled from 5 slice cultures, each. For *N* preparations: CTL, 4; IFN-γ (100 ng/ml, 24 h), 4; unpaired *t*-test. (*D*) Immunohistochemistry with the activation marker CD86 in CTL and IFN-γ. Note the moderate increase in IFN-γ. (*E*) The levels of CD40 mRNA were determined in tissue homogenates pooled from 5 slice cultures, each. For *N* preparations: CTL, 3; IFN-γ (100 ng/ml, 24 h), 4; $P = 0.053$, unpaired *t*-test. All sample images are taken from the

CA3 region (Fig. 3). Note that CD80 and CD86 serve as costimulatory molecules on microglia to maintain T cell stimulation (Satoh et al., 1995).

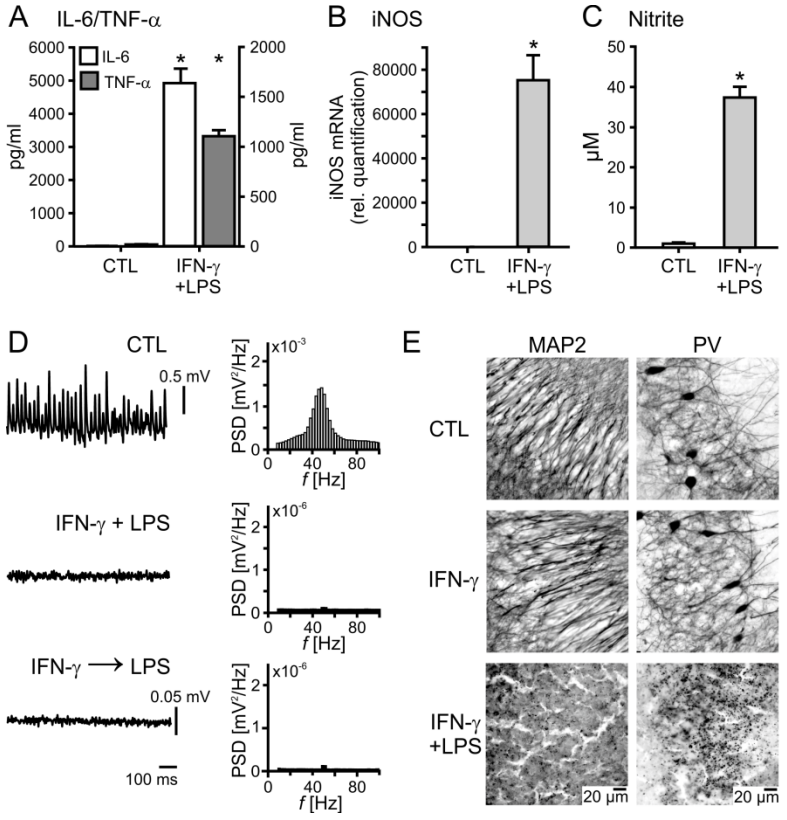

Fig. S2. Inflammatory neurodegeneration during simultaneous and serial exposures to IFN-γ and LPS. Slice cultures were exposed to IFN-γ (100 ng/ml) plus LPS (100 ng/ml) for 72 h (IFN-γ+LPS) or IFN-γ (1000 ng/ml) for 72 h followed by LPS (1000 ng/ml) for 24 h (IFN-γ→LPS). (*A*) IL-6 and TNF-α levels were determined in the culture medium. **P* < 0.001 vs. CTL, unpaired *t*-tests. For *n/N* membranes/preparations: CTL, 4/4; IFN-γ+LPS, 4/4. (*B*) The levels of iNOS mRNA were determined in tissue homogenates pooled from 5 slice cultures, each. **P* < 0.05 vs. CTL, unpaired *t*-test. For *N* preparations: CTL, 2; IFN-γ+LPS, 2. (*C*) The levels of nitrite reflecting nitric oxide (NO) release were determined in the culture medium. **P* < 0.001 vs. CTL, unpaired *t*-test. For *n/N* membranes/preparations: CTL, 5/5; IFN-γ+LPS, 5/5. Note the severalfold higher values in IFN-γ+LPS (*A*-*C*) compared with IFN-γ alone (Fig. 2). (*D*) After exposures to IFN-γ and LPS, electrophysiological recordings were done in the stratum pyramidale of CA3, with acetylcholine (2 μM) and physostigmine (400 nM) present in ACSF.

Sample traces of local field potential recordings and corresponding power spectral density (PSD) calculated from data segments of 5 min. Gamma oscillations were present in 86% (CTL), 0% (IFN-γ+LPS) (I), 0% (IFN-γ+LPS) (II) and 0% (IFN-γ→LPS) of slice cultures. For *n/N* slices/preparations: CTL, 34/8; IFN-γ (10 ng/ml) plus LPS (1000 ng/ml) (I), 26/4; IFN-γ (100 ng/ml) plus LPS (100 ng/ml) (II), 23/4; IFN-γ (1000 ng/ml) followed by LPS (1000 ng/ml), 24/2. Note the complete loss of neuronal activity in IFN-γ+LPS and IFN-γ→LPS. (*E*) Corresponding immunohistochemistry of microtubule-associated protein 2 (MAP2) and parvalbumin (PV) that stains inhibitory interneurons, such as basket cells. Sample images are taken from CA3 (Fig. 3). Note the massive structural damage of neurons in IFN-γ+LPS (whole slice staining).

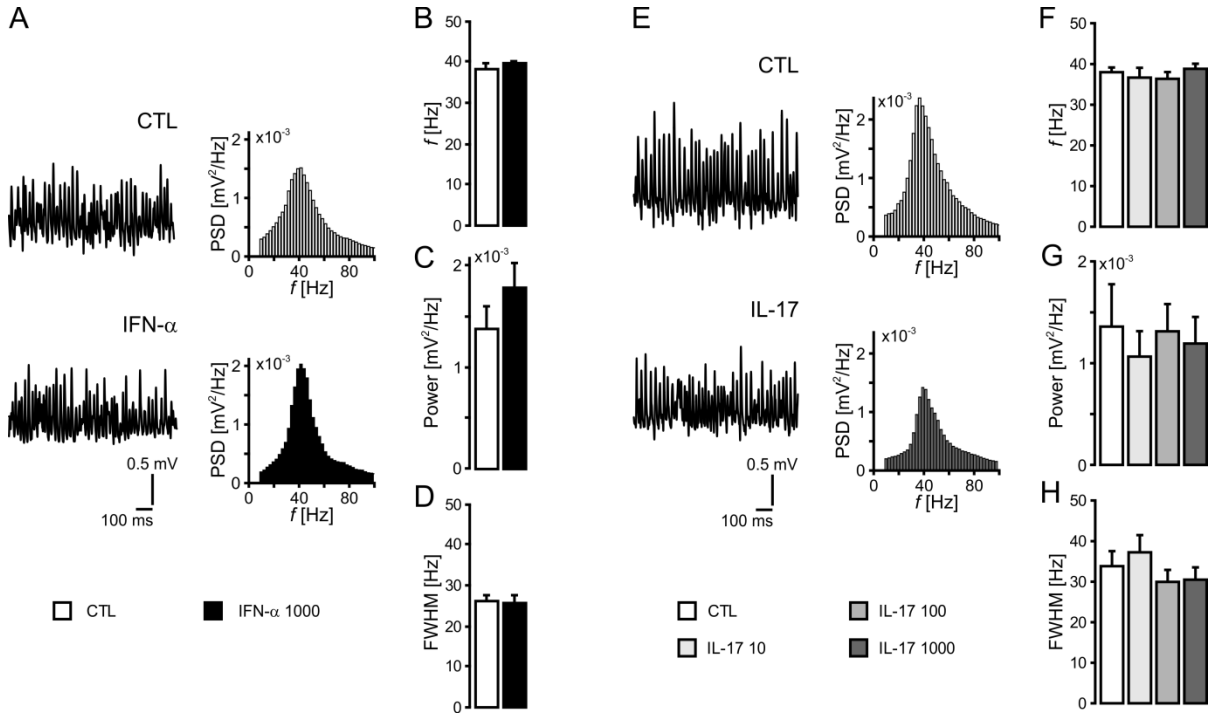

Fig. S3. IFN-α and IL-17 do not affect the properties of gamma oscillations. Slice cultures were exposed to IFN-α (1000 U/ml) or IL-17 at different concentrations (10, 100 and 1000 ng/ml) for 72 h. Electrophysiological recordings were done in the stratum pyramidale of CA3, with acetylcholine (2 µM) and physostigmine (400 nM) present in ACSF. (*A, E*) Sample traces of gamma oscillations and corresponding power spectral density (PSD) (bin size = 2.441 Hz) calculated from data segments of 5 min. (*B, F*) Frequency (*f*), (*C, G*) power, and (*D, H*) FWHM were calculated from power spectral density in naive control (white) and exposed (black and grey shades) slice cultures. For *n/N* slices/preparations: CTL, 20/2; IFN-α (1000 U/ml), 19/2; unpaired *t*-test (*f* and FWHM) and Mann-Whitney Rank Sum Test (power) (*B-D*). CTL, 15/5; IL-17 (10 ng/ml), 14/5; IL-17 (100 ng/ml), 15/5; IL-17 (1000 ng/ml), 15/5; Kruskal-Wallis test with Dunn's post hoc test (*F-H*).

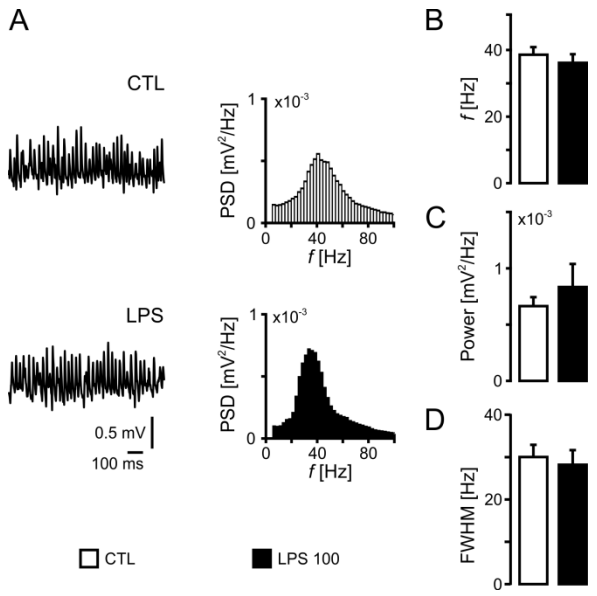

Fig. S4. LPS (100 ng/ml) does not affect the properties of gamma oscillations. Slice cultures were exposed to LPS (100 ng/ml) for 72 h. Electrophysiological recordings were done in the stratum pyramidale of CA3, with acetylcholine (2 µM) and physostigmine (400 nM) present in ACSF. (*A*) Sample traces of gamma oscillations and corresponding power spectral density (PSD) (bin size = 2.441 Hz) calculated from data segments of 5 min. (*B*) Frequency (*f*), (*C*) power, and (*D*) FWHM were calculated from power spectral density (PSD) in naive control (white) and exposed (black) slice cultures. For *n/N* slices/preparations: CTL, 16/5; LPS, 17/5; unpaired *t*-test (*f* and FWHM) and Mann-Whitney Rank Sum Test (power).

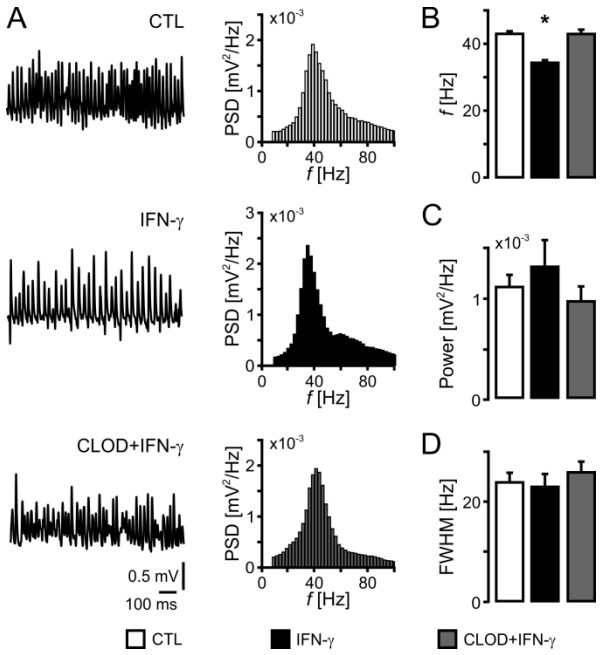

Fig. S5. Microglia-mediated slowing of gamma oscillations. Slice cultures were exposed to IFN-γ (1000 ng/ml) and clodronate (100 µg/ml) plus IFN-γ (1000 ng/ml) (CLOD+IFN-γ) for 72 h. Electrophysiological recordings were done in the stratum pyramidale of CA3, with acetylcholine (2 µM) and physostigmine (400 nM) present in ACSF. (*A*) Sample traces of gamma oscillations and corresponding power spectral density (PSD) (bin size = 2.441 Hz) calculated from data segments of 5 min. (*B*) Frequency (*f*), (*C*) power, and (*D*) FWHM were calculated from power spectral density in naive control (white) and exposed (black, grey) slice cultures. For *n/N* slices/preparations: CTL, 25/5; IFN-γ, 18/4; CLOD+IFN-γ, 12/5. **P* < 0.05 vs. CTL and CLOD+IFN-γ, Kruskal-Wallis test with Dunn's post hoc test.

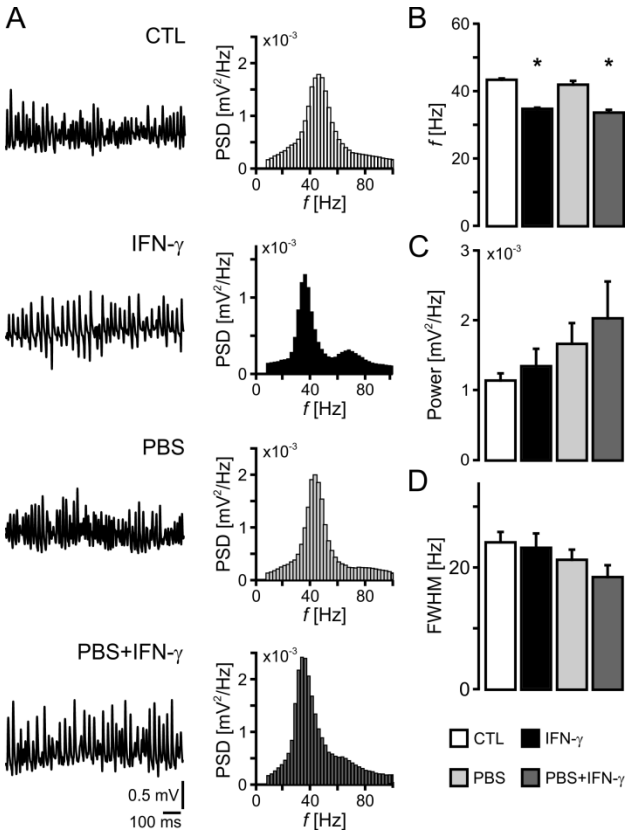

Fig. S6. Control experiments with PBS-containing liposomes. Slice cultures were exposed to IFN-γ (1000 ng/ml), PBS-containing liposomes (100 µg/ml) (PBS), and PBS-containing liposomes plus IFN-γ (PBS+IFN-γ) for 72 h. After exposure, local field potentials were recorded in the stratum pyramidale of CA3 in the slice cultures, with acetylcholine (2 µM) and physostigmine (400 nM) present in ACSF. Sample traces of the local field potential and corresponding power spectral density (PSD) (bin size = 2.441 Hz) calculated from data segments of 5 min in CTL, IFN-γ, PBS and PBS+IFN-γ. For *n/N* slices/preparations: CTL, 25/5; IFN-γ, 18/4; PBS, 12/4; PBS+IFN-γ, 12/4. **P* < 0.001 vs. CTL, Kruskal-Wallis test with Dunn's post hoc test. Note the clear decline in the frequency of gamma oscillations in IFN-γ and in PBS+IFN-γ.

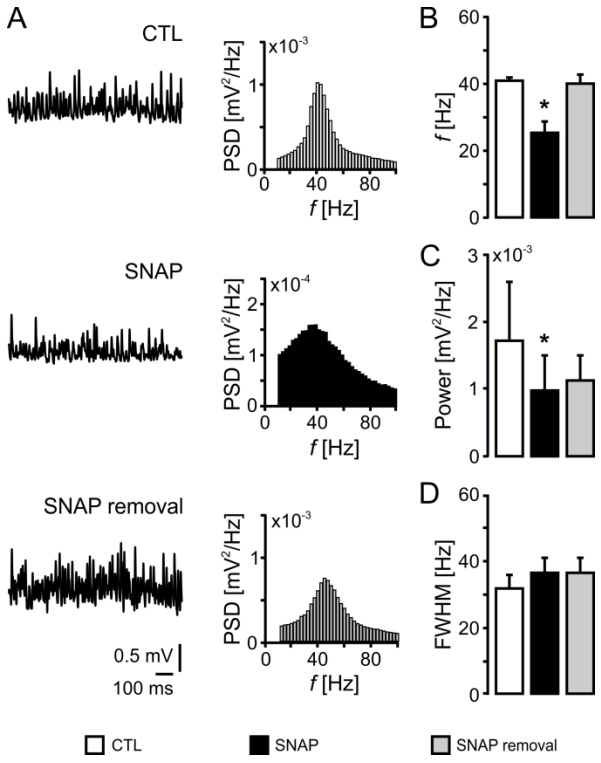

Fig. S7. Acute effects of the NO-donor SNAP on gamma oscillations. Electrophysiological recordings were done in the stratum pyramidale of CA3 in naive (untreated) slice cultures, with acetylcholine (2 µM) and physostigmine (400 nM) present in ACSF. (*A*) Sample traces of the local field potential and corresponding power spectral density (PSD) (bin size = 2.441 Hz) calculated from data segments of 5 min in slice cultures expressing gamma oscillations in control condition (CTL), during acute application of SNAP (100 µM) and after SNAP removal. (*B*) Frequency (*f*), (*C*) power, and (*D*) FWHM were calculated from power spectral density in CTL (white), SNAP (black) and after SNAP removal (grey). For *n/N* slices/preparations: 17/7. **P* < 0.05 vs. CTL, Friedman test with Dunn's post hoc test (*f*, power), one-way repeated-measures ANOVA with Holm-Sidak's post hoc test (FWHM).

SI References

Ajmone-Cat MA, Mancini M, De Simone R, Cilli P, Minghetti L. Microglial polarization and plasticity: evidence from organotypic hippocampal slice cultures. Glia. 2013 Oct;61(10):1698-711. doi: 10.1002/glia.22550. Epub 2013 Aug 5.

Arancio O, Kiebler M, Lee CJ, Lev-Ram V, Tsien RY, Kandel ER, Hawkins RD. Nitric oxide acts directly in the presynaptic neuron to produce long-term potentiation in cultured hippocampal neurons. Cell. 1996 Dec 13;87(6):1025-35.

Bahr BA, Kessler M, Rivera S, Vanderklish PW, Hall RA, Mutneja MS, Gall C, Hoffman KB. Stable maintenance of glutamate receptors and other synaptic components in long-term hippocampal slices. Hippocampus. 1995;5(5):425-39.

Bell RD, Zlokovic BV. Neurovascular mechanisms and blood-brain barrier disorder in Alzheimer's disease. Acta Neuropathol. 2009 Jul;118(1):103-13. doi: 10.1007/s00401-009-0522-3. Epub 2009 Mar 25.

Bolaños JP, Delgado-Esteban M, Herrero-Mendez A, Fernandez-Fernandez S, Almeida A. Regulation of glycolysis and pentose-phosphate pathway by nitric oxide: impact on neuronal survival. Biochim Biophys Acta. 2008 Jul-Aug;1777(7-8):789-93. doi: 10.1016/j.bbabio.2008.04.011. Epub 2008 Apr 13.

Bolaños JP, Peuchen S, Heales SJ, Land JM, Clark JB. Nitric oxide-mediated inhibition of the mitochondrial respiratory chain in cultured astrocytes. J Neurochem. 1994 Sep;63(3):910-6.

Brorson JR1, Schumacker PT, Zhang H. Nitric oxide acutely inhibits neuronal energy production. J Neurosci. 1999 Jan 1;19(1):147-58.

Brown GC, Cooper CE. Nanomolar concentrations of nitric oxide reversibly inhibit synaptosomal respiration by competing with oxygen at cytochrome oxidase. FEBS Lett. 1994 Dec 19;356(2-3):295-8.

Brown GC, Neher JJ. Inflammatory neurodegeneration and mechanisms of microglial killing of neurons. Mol Neurobiol. 2010 Jun;41(2-3):242-7. doi: 10.1007/s12035-010-8105-9. Epub 2010 Mar 2.

Brown GC, Vilalta A. How microglia kill neurons. Brain Res. 2015 Dec 2;1628(Pt B):288-297. doi: 10.1016/j.brainres.2015.08.031. Epub 2015 Sep 2. Review.

Cleeter MW, Cooper JM, Darley-Usmar VM, Moncada S, Schapira AH. Reversible inhibition of cytochrome c oxidase, the terminal enzyme of the mitochondrial respiratory chain, by nitric oxide. Implications for neurodegenerative diseases. FEBS Lett. 1994 May 23;345(1):50-4.

Colton CA, Yao J, Keri JE, Gilbert D. Regulation of microglial function by interferons. J Neuroimmunol. 1992 Sep;40(1):89-98.

Colton CA. Heterogeneity of microglial activation in the innate immune response in the brain. J Neuroimmune Pharmacol. 2009 Dec;4(4):399-418. doi: 10.1007/s11481-009-9164-4. Epub 2009 Aug 5. Review.

Daneman R, Prat A. The blood-brain barrier. Cold Spring Harb Perspect Biol. 2015 Jan 5;7(1):a020412. doi: 10.1101/cshperspect.a020412.

Dejanovic B, Schwarz G. Neuronal nitric oxide synthase-dependent S-nitrosylation of gephyrin regulates gephyrin clustering at GABAergic synapses. J Neurosci. 2014 Jun 4;34(23):7763-8. doi: 10.1523/JNEUROSCI.0531-14.2014.

Dendrou CA, Fugger L, Friese MA. Immunopathology of multiple sclerosis. Nat Rev Immunol. 2015 Sep 15;15(9):545-58. doi: 10.1038/nri3871.

Ding M, St Pierre BA, Parkinson JF, Medberry P, Wong JL, Rogers NE, Ignarro LJ, Merrill JE. Inducible nitric-oxide synthase and nitric oxide production in human fetal astrocytes and microglia. A kinetic analysis. J Biol Chem. 1997 Apr 25;272(17):11327-35.

Duport S, Garthwaite J. Pathological consequences of inducible nitric oxide synthase expression in hippocampal slice cultures. Neuroscience. 2005;135(4):1155-66. Epub 2005 Sep 13.

Feil R, Kleppisch T. NO/cGMP-dependent modulation of synaptic transmission. Handb Exp Pharmacol. 2008;(184):529-60.

Fischer Y, Wittner L, Freund TF, Gähwiler BH. Simultaneous activation of gamma and theta network oscillations in rat hippocampal slice cultures. J Physiol. 2002 Mar 15;539(Pt 3):857-68.

Frere S, Slutsky I. Alzheimer's Disease: From Firing Instability to Homeostasis Network Collapse. Neuron. 2018 Jan 3;97(1):32-58. doi: 10.1016/j.neuron.2017.11.028.

Gasulla J, Calvo DJ. Enhancement of tonic and phasic GABAergic currents following nitric oxide synthase inhibition in hippocampal CA1 pyramidal neurons. Neurosci Lett. 2015 Mar 17;590:29-34. doi: 10.1016/j.neulet.2015.01.058. Epub 2015 Jan 27.

Gillespie AK, Jones EA, Lin YH, Karlsson MP, Kay K, Yoon SY, Tong LM, Nova P, Carr JS, Frank LM, Huang Y. Apolipoprotein E4 Causes Age-Dependent Disruption of Slow Gamma Oscillations during Hippocampal Sharp-Wave Ripples. Neuron. 2016 May 18;90(4):740-51. doi: 10.1016/j.neuron.2016.04.009. Epub 2016 May 5.

Giunti D, Borsellino G, Benelli R, Marchese M, Capello E, Valle MT, Pedemonte E, Noonan D, Albini A, Bernardi G, Mancardi GL, Battistini L, Uccelli A. Phenotypic and functional analysis of T cells homing into the CSF of subjects with inflammatory diseases of the CNS. J Leukoc Biol. 2003 May;73(5):584-90.

Grau V, Herbst B, van der Meide PH, Steiniger B. Activation of microglial and endothelial cells in the rat brain after treatment with interferon-gamma in vivo. Glia. 1997 Mar;19(3):181-9.

Hailer NP, Jarhult JD, Nitsch R. Resting microglial cells in vitro: analysis of morphology and adhesion molecule expression in organotypic hippocampal slice cultures. Glia. 1996 Dec;18(4):319-31.

Hájos N, Paulsen O. Network mechanisms of gamma oscillations in the CA3 region of the hippocampus. Neural Netw. 2009 Oct;22(8):1113-9. doi: 10.1016/j.neunet.2009.07.024. Epub 2009 Jul 22.

Hanisch UK, Kettenmann H. Microglia: active sensor and versatile effector cells in the normal and pathologic brain. Nat Neurosci. 2007 Nov;10(11):1387-94.

Hardingham N, Dachtler J, Fox K. The role of nitric oxide in pre-synaptic plasticity and homeostasis. Front Cell Neurosci. 2013 Oct 31;7:190. doi: 10.3389/fncel.2013.00190.

Heesen C, Nawrath L, Reich C, Bauer N, Schulz KH, Gold SM. Fatigue in multiple sclerosis: an example of cytokine mediated sickness behaviour? J Neurol Neurosurg Psychiatry. 2006 Jan;77(1):34-9.

Herrera-Molina R, Flores B, Orellana JA, von Bernhardi R. Modulation of interferon-γ-induced glial cell activation by transforming growth factor β1: a role for STAT1 and MAPK pathways. J Neurochem. 2012 Oct;123(1):113-23. doi: 10.1111/j.1471-4159.2012.07887.x. Epub 2012 Aug 22.

Hoos MD, Vitek MP, Ridnour LA, Wilson J, Jansen M, Everhart A, Wink DA, Colton CA. The impact of human and mouse differences in NOS2 gene expression on the brain's redox and immune environment. Mol Neurodegener. 2014 Nov 17;9:50. doi: 10.1186/1750-1326-9-50.

Hu S, Sheng WS, Peterson PK, Chao CC. Cytokine modulation of murine microglial cell superoxide production. Glia. 1995 Jan;13(1):45-50.

Huchzermeyer C, Berndt N, Holzhütter HG, Kann O. Oxygen consumption rates during three different neuronal activity states in the hippocampal CA3 network. J Cereb Blood Flow Metab. 2013 Feb;33(2):263-71. doi: 10.1038/jcbfm.2012.165. Epub 2012 Nov 21.

Hyman BT, Trojanowski JQ. Consensus recommendations for the postmortem diagnosis of Alzheimer disease from the National Institute on Aging and the Reagan Institute Working Group on diagnostic criteria for the neuropathological assessment of Alzheimer disease. J Neuropathol Exp Neurol. 1997 Oct;56(10):1095-7.

Inserra A, Mastronardi CA, Rogers G, Licinio J, Wong ML. Neuroimmunomodulation in Major Depressive Disorder: Focus on Caspase 1, Inducible Nitric Oxide Synthase, and Interferon-Gamma. Mol Neurobiol. 2018 Oct 10. doi: 10.1007/s12035-018-1359-3. [Epub ahead of print]

Johnstone VP, Raymond CR. A protein synthesis and nitric oxide-dependent presynaptic enhancement in persistent forms of long-term potentiation. Learn Mem. 2011 Sep 20;18(10):625-33. doi: 10.1101/lm.2245911. Print 2011 Oct.

Kann O. The interneuron energy hypothesis: Implications for brain disease. Neurobiol Dis. 2016 Jun;90:75-85. doi: 10.1016/j.nbd.2015.08.005. Epub 2015 Aug 16. Review.

Kann O, Huchzermeyer C, Kovács R, Wirtz S, Schuelke M. Gamma oscillations in the hippocampus require high complex I gene expression and strong functional performance of mitochondria. Brain. 2011 Feb;134(Pt 2):345-58. doi: 10.1093/brain/awq333. Epub 2010 Dec 22.

Kann O, Schuchmann S, Buchheim K, Heinemann U. Coupling of neuronal activity and mitochondrial metabolism as revealed by NAD(P)H fluorescence signals in organotypic hippocampal slice cultures of the rat. Neuroscience. 2003;119(1):87-100.

Klein RS, Garber C, Howard N. Infectious immunity in the central nervous system and brain function. Nat Immunol. 2017 Feb;18(2):132-141. doi: 10.1038/ni.3656. Epub 2017 Jan 16.

Kothur K, Wienholt L, Brilot F, Dale RC. CSF cytokines/chemokines as biomarkers in neuroinflammatory CNS disorders: A systematic review. Cytokine. 2016 Jan;77:227-37. doi: 10.1016/j.cyto.2015.10.001. Epub 2015 Oct 14.

Lange MD, Doengi M, Lesting J, Pape HC, Jüngling K. Heterosynaptic long-term potentiation at interneuron-principal neuron synapses in the amygdala requires nitric oxide signalling. J Physiol. 2012 Jan 1;590(1):131-43. doi: 10.1113/jphysiol.2011.221317. Epub 2011 Oct 31.

Lee SC, Dickson DW, Liu W, Brosnan CF. Induction of nitric oxide synthase activity in human astrocytes by interleukin-1 beta and interferon-gamma. J Neuroimmunol. 1993 Jul;46(1-2):19-24.

Lipton SA, Choi YB, Pan ZH, Lei SZ, Chen HS, Sucher NJ, Loscalzo J, Singel DJ, Stamler JS. A redox-based mechanism for the neuroprotective and neurodestructive effects of nitric oxide and related nitroso-compounds. Nature. 1993 Aug 12;364(6438):626-32.

Lynch MA. The impact of neuroimmune changes on development of amyloid pathology; relevance to Alzheimer's disease. Immunology. 2014 Mar;141(3):292-301. doi: 10.1111/imm.12156. Review.

Mably AJ, Colgin LL. Gamma oscillations in cognitive disorders. Curr Opin Neurobiol. 2018 Oct;52:182-187. doi: 10.1016/j.conb.2018.07.009. Epub 2018 Aug 16.

Mably AJ, Gereke BJ, Jones DT, Colgin LL. Impairments in spatial representations and rhythmic coordination of place cells in the 3xTg mouse model of Alzheimer's disease. Hippocampus. 2017 Apr;27(4):378-392. doi: 10.1002/hipo.22697. Epub 2017 Jan 16.

McKhann GM, Knopman DS, Chertkow H, Hyman BT, Jack CR Jr, Kawas CH, Klunk WE, Koroshetz WJ, Manly JJ, Mayeux R, Mohs RC, Morris JC, Rossor MN, Scheltens P, Carrillo MC, Thies B, Weintraub S, Phelps CH. The diagnosis of dementia due to Alzheimer's disease: recommendations from the National Institute on Aging-Alzheimer's Association workgroups on diagnostic guidelines for Alzheimer's disease. Alzheimers Dement. 2011 May;7(3):263-9. doi: 10.1016/j.jalz.2011.03.005. Epub 2011 Apr 21.

McManus RM, Heneka MT. Role of neuroinflammation in neurodegeneration: new insights. Alzheimers Res Ther. 2017 Mar 4;9(1):14. doi: 10.1186/s13195-017-0241-2.

McManus RM, Higgins SC, Mills KH, Lynch MA. Respiratory infection promotes T cell infiltration and amyloid-β deposition in APP/PS1 mice. Neurobiol Aging. 2014 Jan;35(1):109-21. doi: 10.1016/j.neurobiolaging.2013.07.025. Epub 2013 Aug 29.

Miller BJ, Buckley P, Seabolt W, Mellor A, Kirkpatrick B. Meta-analysis of cytokine alterations in schizophrenia: clinical status and antipsychotic effects. Biol Psychiatry. 2011 Oct 1;70(7):663-71. doi: 10.1016/j.biopsych.2011.04.013. Epub 2011 Jun 8.

Monson NL, Ireland SJ, Ligocki AJ, Chen D, Rounds WH, Li M, Huebinger RM, Munro Cullum C, Greenberg BM, Stowe AM, Zhang R. Elevated CNS inflammation in patients with preclinical Alzheimer's disease. J Cereb Blood Flow Metab. 2014 Jan;34(1):30-3. doi: 10.1038/jcbfm.2013.183.

Montagne A, Barnes SR, Sweeney MD, Halliday MR, Sagare AP, Zhao Z, Toga AW, Jacobs RE, Liu CY, Amezcua L, Harrington MG, Chui HC, Law M, Zlokovic BV. Blood-brain barrier breakdown in the aging human hippocampus. Neuron. 2015 Jan 21;85(2):296-302. doi: 10.1016/j.neuron.2014.12.032.

Morán M, Moreno-Lastres D, Marín-Buera L, Arenas J, Martín MA, Ugalde C. Mitochondrial respiratory chain dysfunction: implications in neurodegeneration. Free Radic Biol Med. 2012 Aug 1;53(3):595-609. doi: 10.1016/j.freeradbiomed.2012.05.009. Epub 2012 May 14. Review.

Mosser DM, Edwards JP. Exploring the full spectrum of macrophage activation. Nat Rev Immunol. 2008 Dec;8(12):958-69. doi: 10.1038/nri2448. Review.

Na KS, Jung HY, Kim YK. The role of pro-inflammatory cytokines in the neuroinflammation and neurogenesis of schizophrenia. Prog Neuropsychopharmacol Biol Psychiatry. 2014 Jan 3;48:277-86. doi: 10.1016/j.pnpbp.2012.10.022. Epub 2012 Nov 1.

Neitz A, Mergia E, Imbrosci B, Petrasch-Parwez E, Eysel UT, Koesling D, Mittmann T. Postsynaptic NO/cGMP increases NMDA receptor currents via hyperpolarization-activated cyclic nucleotide-gated channels in the hippocampus. Cereb Cortex. 2014 Jul;24(7):1923-36. doi: 10.1093/cercor/bht048. Epub 2013 Feb 28.

Neumann H, Boucraut J, Hahnel C, Misgeld T, Wekerle H. Neuronal control of MHC class II inducibility in rat astrocytes and microglia. Eur J Neurosci. 1996 Dec;8(12):2582-90.

Pan W, Banks WA, Kastin AJ. Permeability of the blood-brain and blood-spinal cord barriers to interferons. J Neuroimmunol. 1997 Jun;76(1-2):105-11.

Papageorgiou IE, Lewen A, Galow LV, Cesetti T, Scheffel J, Regen T, Hanisch UK, Kann O. TLR4-activated microglia require IFN-γ to induce severe neuronal dysfunction and death in situ. Proc Natl Acad Sci U S A. 2016 Jan 5;113(1):212-7. doi: 10.1073/pnas.1513853113. Epub 2015 Dec 22.

Pawate S, Shen Q, Fan F, Bhat NR. Redox regulation of glial inflammatory response to lipopolysaccharide and interferongamma. J Neurosci Res. 2004 Aug 15;77(4):540-51.

Peterson PK, Hu S, Anderson WR, Chao CC. Nitric oxide production and neurotoxicity mediated by activated microglia from human versus mouse brain. J Infect Dis. 1994 Aug;170(2):457-60.

Prinz M, Priller J. The role of peripheral immune cells in the CNS in steady state and disease. Nat Neurosci. 2017 Feb;20(2):136-144. doi: 10.1038/nn.4475. Epub 2017 Jan 16. Review.

Ransohoff RM. How neuroinflammation contributes to neurodegeneration. Science. 2016 Aug 19;353(6301):777-83. doi: 10.1126/science.aag2590.

Ransohoff RM, Perry VH. Microglial physiology: unique stimuli, specialized responses. Annu Rev Immunol. 2009;27:119-45. doi: 10.1146/annurev.immunol.021908.132528.

Rogers J, Luber-Narod J, Styren SD, Civin WH. Expression of immune system-associated antigens by cells of the human central nervous system: relationship to the pathology of Alzheimer's disease. Neurobiol Aging. 1988 Jul-Aug;9(4):339-49.

Roy DS, Arons A, Mitchell TI, Pignatelli M, Ryan TJ, Tonegawa S. Memory retrieval by activating engram cells in mouse models of early Alzheimer's disease. Nature. 2016 Mar 24;531(7595):508-12. doi: 10.1038/nature17172. Epub 2016 Mar 16.

Satoh J, Lee YB, Kim SU. T-cell costimulatory molecules B7-1 (CD80) and B7-2 (CD86) are expressed in human microglia but not in astrocytes in culture. Brain Res. 1995 Dec 15;704(1):92-6.

Schneider J, Berndt N, Papageorgiou IE, Maurer J, Bulik S, Both M, Draguhn A, Holzhütter HG, Kann O. Local oxygen homeostasis during various neuronal network activity states in the mouse hippocampus. J Cereb Blood Flow Metab. 2017 Jan 1:271678X17740091. doi: 10.1177/0271678X17740091. [Epub ahead of print]

Schneider J, Lewen A, Ta TT, Galow LV, Isola R, Papageorgiou IE, Kann O. A reliable model for gamma oscillations in hippocampal tissue. J Neurosci Res. 2015 Jul;93(7):1067-78. doi: 10.1002/jnr.23590. Epub 2015 Mar 24.

Schneider CA, Rasband WS, Eliceiri KW. NIH Image to ImageJ: 25 years of image analysis. Nat Methods. 2012 Jul;9(7):671-5.

Spencer NG, Schilling T, Miralles F, Eder C. Mechanisms Underlying Interferon-γ-Induced Priming of Microglial Reactive Oxygen Species Production. PLoS One. 2016 Sep 6;11(9):e0162497. doi: 10.1371/journal.pone.0162497. eCollection 2016.

Stoppini L, Buchs PA, Muller D. A simple method for organotypic cultures of nervous tissue. J Neurosci Methods. 1991 Apr;37(2):173-82.

Szabadits E, Cserép C, Ludányi A, Katona I, Gracia-Llanes J, Freund TF, Nyíri G. Hippocampal GABAergic synapses possess the molecular machinery for retrograde nitric oxide signaling. J Neurosci. 2007 Jul 25;27(30):8101-11.

Togo T, Akiyama H, Iseki E, Kondo H, Ikeda K, Kato M, Oda T, Tsuchiya K, Kosaka K. Occurrence of T cells in the brain of Alzheimer's disease and other neurological diseases. J Neuroimmunol. 2002 Mar;124(1-2):83-92.

van de Haar HJ, Burgmans S, Jansen JF, van Osch MJ, van Buchem MA, Muller M, Hofman PA, Verhey FR, Backes WH. Blood-Brain Barrier Leakage in Patients with Early Alzheimer Disease. Radiology. 2016 Nov;281(2):527-535. Epub 2016 May 31.

Vinet J, Weering HR, Heinrich A, Kälin RE, Wegner A, Brouwer N, Heppner FL, Rooijen Nv, Boddeke HW, Biber K. Neuroprotective function for ramified microglia in hippocampal excitotoxicity. J Neuroinflammation. 2012 Jan 31;9:27. doi: 10.1186/1742-2094-9-27.

West AR, Galloway MP, Grace AA. Regulation of striatal dopamine neurotransmission by nitric oxide: effector pathways and signaling mechanisms. Synapse. 2002 Jun 15;44(4):227-45.

Wink DA, Hanbauer I, Krishna MC, DeGraff W, Gamson J, Mitchell JB. Nitric oxide protects against cellular damage and cytotoxicity from reactive oxygen species. Proc Natl Acad Sci U S A. 1993 Nov 1;90(21):9813-7.